Kinetics of the Heterogeneous Reaction of HNO_3 with NaCl: Effect of Water Vapor

Julia A. Davies and R. Anthony Cox*

Centre for Atmospheric Science, Department of Chemistry, University of Cambridge, Lensfield Road, Cambridge, CB2 1EW, U.K.

Received: May 5, 1998; In Final Form: July 22, 1998

The kinetics of uptake of gaseous HNO_3 on thin films and crystallite grains of NaCl has been studied in a coated wall tubular flow reactor coupled to a quadrupole mass spectrometer. A rapid gas−solid reaction occurs with release of gaseous HCl. Uptake coefficients were measured at room temperature with a range of partial pressures of HNO_3 and H_2O in the flow tube. γ values decreased with increasing HNO_3 concentration (4×10^{11} to 700×10^{11} molecule cm^{-3}) and increased with H_2O over the range 2×10^{-4} to 10 mbar. The results were interpreted in terms of a mechanism of the reaction $HNO_3(g) + NaCl(s) \rightarrow HCl(g) + NaNO_3(s)$, which involves ionization of adsorbed HNO_3 molecules aided by surface-adsorbed water followed by reaction of H_3O^+ with Cl^- and desorption of product HCl molecules. The results allow estimation of the reactive uptake coefficient for HNO_3 on sea salt aerosol under atmospheric conditions.

1. Introduction

Although atmospheric oxidation in the troposphere is primarily driven by HO_x radicals, there is emerging evidence that in the marine environment and in polar regions, halogen atoms, Cl and Br, could play a significant role in oxidation chemistry.[1−4] The main gaseous inorganic chlorine carrier in the troposphere is HCl. The amounts of HCl present in the marine boundary layer appear to be larger by an order of magnitude than can be accounted for by gas-phase oxidation of organic halides.[5] Another potential source of halogens is chemical reactions of sea salt aerosols, which are generated by wave-breaking on the ocean surface and when generated are composed mainly of NaCl.

The quantity of halogen salts injected into the atmosphere in the form of sea salt is very large. Observations made over many years have shown a deficit in the halide ions Cl^- and Br^- relative to the bulk seawater ratio of X^-/Na^+. The deficit in Cl^- is more noticeable in the smaller size fraction of the marine aerosol and in coastal regions, and it is believed to arise from release of halogen from the salt particles or droplets in the form of volatile chlorine-containing gases such as HCl.[6,7]

The form and mechanism of halogen release is not well established. Several mechanisms have been proposed, which fall into three categories: (1) acid−base reaction, where HCl is released by reaction of a strong acid[8] (HNO_3 or H_2SO_4) with NaCl, for example,

$$HNO_3\,(g) + NaCl\,(s) \rightarrow HCl\,(g) + NaNO_3\,(s)$$

(2) oxidation by nitrogen oxides,[9,10] resulting in formation of gaseous nitroxy halide species, for example,

$$N_2O_5\,(g) + NaCl\,(s) \rightarrow ClNO_2\,(g) + NaNO_3\,(s)$$

(3) redox reactions involving other oxidizing agents such as O_3,[11] OH, or hypohalous acids,[12] leading to the release of elemental halogen or interhalogen, for example,

$$HOBr\,(g) + NaCl\,(s) \rightarrow BrCl\,(g) + NaOH\,(s)$$

All these reactions can occur in principle on solid NaCl surfaces or in concentrated aqueous salt solutions near or above the deliquescent point of NaCl. Field observations of the ionic composition of the marine aerosol provide strong evidence that HCl can be released by strong acids H_2SO_4 and HNO_3. This is particularly important in coastal regions where polluted air containing HNO_3, SO_2, and nitrogen oxides advects into the marine environment.[13] There is an important need to investigate the kinetics and mechanism of these proposed reactions in the laboratory in order to assess their atmospheric importance.

The kinetics of the reaction of HNO_3 with solid NaCl has been investigated by several groups. Reaction rates were reported as reactive uptake coefficients γ, which represent the fraction of surface collisions of gaseous HNO_3 molecules that lead to the overall reaction. Fenter et al.[14] observed the kinetics of uptake of gaseous HNO_3 on salt powders in a Teflon coated low-pressure Knudsen cell flow reactor, with mass spectrometric detection. They report quantitative conversion of HNO_3 to HCl with a value of the uptake coefficient of $\gamma = (2.8 \pm 0.3) \times 10^{-2}$ at 298 K. At about the same time Laux et al.[15] used X-ray photoelectron spectroscopy to follow the formation of nitrate on surfaces of single crystals of NaCl and obtained a much lower value of $\gamma = (4 \pm 2) \times 10^{-4}$ at 298 K.

In later work Fenter et al.[16] reported values of γ ranging from 1.3×10^{-2} to 5.5×10^{-2} depending on surface presentation, including polished salt windows, spray coated samples, and grains. The rate of uptake depended only on the external geometric surface area of the sample, but saturation effects were observed at high HNO_3 concentration. The quoted values of γ were for conditions of low exposure, i.e., short reaction time and low [HNO_3].

Leu et al.[17] investigated the kinetics of reaction 1 over the temperature range 223−296 K in a flow tube reactor coupled to a quadropole mass spectrometer. The NaCl sample consisted of 0.44 mm diameter grains situated on the flat bottom surface of the flow reactor. A substantial correction to the uptake rates was made for pore diffusion effects. HNO_3 concentrations in the range $(0.2-98) \times 10^{10}$ molecules cm^{-3} were employed. The average value of γ for low HNO_3 concentrations was (1.3 ±

S1089-5639(98)02134-3 CCC: $15.00
Published on Web 09/09/1998

0.4) $\times 10^{-2}$ at 296 K and $\sim 8 \times 10^{-3}$ at 223 K, but the uptake coefficients decreased with increasing [HNO_3], which was attributed to surface deactivation, as observed by Fenter et al. Small amounts of water vapor (up to 6.5×10^{12} molecule cm^{-3}) did not significantly influence uptake rate. The mechanism changed from heterogeneous reaction forming gaseous HCl at 296 K to predominantly reversible adsorption at 223 K, which was assumed to be physisorption.

Beichert and Finlayson-Pitts[18] also studied the reaction of HNO_3 with various NaCl crystals and powders, using a low-pressure Knudsen cell and mass spectrometric detection. No uptake or reaction of HNO_3 was observed on single crystals of NaCl, but on polycrystalline materials a rapid initial uptake with production of gaseous HCl was observed followed by a constant uptake rate with a reaction probability of $(1.4 \pm 0.6) \times 10^{-2}$ independent of [HNO_3] in the range of $(3.0-35.0) \times 10^{-12}$ molecules cm^{-3}. They investigated the isotopic composition of the HCl product using isotopically labeled DNO_3 or D_2O in the preparation of the salt sample. The results demonstrated clearly that water absorbed on the surface played a key role in the reaction. A model for HNO_3 uptake and reaction was proposed involving a layer of strongly absorbed water, which was postulated as located at defect sites on the crystal surfaces.

Although there is apparently good agreement between the reported values of γ, there are a number of inconsistencies in the reported data when the effects of surface saturation and surface presentation are considered. Moreover, previous studies of the reaction of HNO_3 with solid NaCl have been conducted with very low partial pressures of H_2O present, mainly because of constraints on the experimental systems used. In view of the apparently important role of water vapor in the heterogeneous reaction forming HCl, it is important to establish the influence of water vapor on the uptake kinetics at partial pressures more comparable with those present in the lower atmosphere. Absorption isotherms for H_2O on NaCl surfaces[19-21,34] show that at room temperature monolayer coverage of the surface is obtained at an H_2O partial pressure of about 10 mbar, corresponding to $\sim$30% relative humidity (RH), i.e., well below the deliquescence point for NaCl (78% RH). Therefore, the adsorption and surface reaction rate of HNO_3 on salt could be modified by changing humidity in this regime.

In the present paper we report a study of the uptake of HNO_3 on salt films and crystallite grains in a coated wall tubular flow reactor coupled to a quadrupole mass spectrometer. The experiments were performed at room temperature (297 ± 2 K) using a range of partial pressures of HNO_3 and H_2O in the flow tube, with the aim of further elucidation of the mechanisms of the reaction and establishment of the reactive uptake coefficient for HNO_3 on sea salt aerosol under atmospheric conditions.

2. Experimental Section

General Description of Apparatus. A conventional fast flow system has been constructed to investigate the kinetics of heterogeneous reactions by monitoring the changes in composition of the gas after exposure to specific coatings on the flow tube wall. It consists of a Pyrex tubular reactor mounted vertically below a differentially pumped molecular-beam-sampling quadrupole mass spectrometer (Hiden HAL RGA301) as illustrated in Figure 1. The reactor is 90 cm in length and 1.9 cm i.d. A cylindrical Pyrex inner tube, 75 cm long and 1.44 cm i.d., is coated internally with the substrate of interest, in this case NaCl, and then inserted inside the flow reactor. This provides the reactive site for the kinetic measurements.

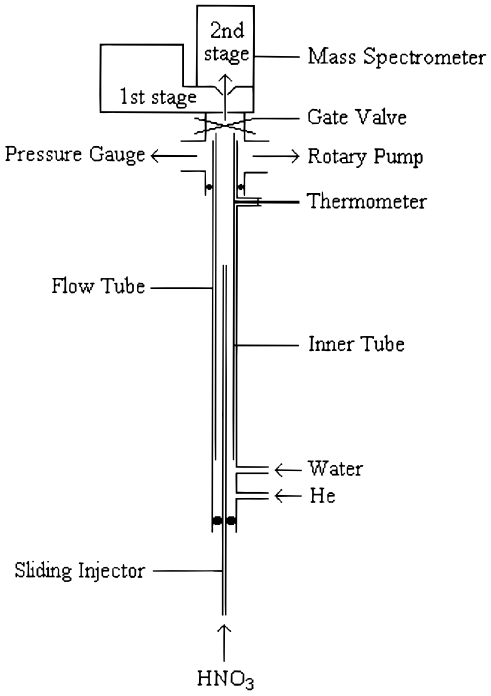

Figure 1. Schematic diagram of the flow system with molecular-beam-sampling mass spectrometer.

The carrier gas, He (Messer Griesheim, grade 5.0), was injected through a side inlet at the upstream end of the flow reactor. In the experiments performed at various water vapor pressures, a continuous flow of water vapor was provided via a second side inlet connected to a Pyrex vessel containing high-purity water. The reactant, HNO_3, was injected into the flow reactor through a 100 cm long sliding injector made of Pyrex, 6 mm o.d., 4 mm i.d., the position of which along the axis of the reactor was adjusted manually. Continuous flow along the reactor, at a constant velocity, was achieved using a 25 $m^3\ h^{-1}$ rotary pump (Leybold Trivac D25B) connected to the upstream end of the flow reactor via a four-way cross-piece (40 mm i.d.) fabricated of aluminum. The total pressure in the reactor was measured by a Baratron gauge (0−100 mbar, Edwards model 600 Barocel) located on the second horizontal port on the cross-piece. The flow rate of He was controlled using a calibrated mass flow meter (Hastings) and a control unit (MKS model 261). The rotary pump was throttled to achieve the desired flow velocity along the flow reactor ($v = M/(PA)$, where v is the flow velocity, M is the mass flow rate, P is the pressure, and A is the cross-sectional area of the flow reactor).

A gate valve was used to isolate the mass spectrometer from the flow reactor so that a new substrate surface may be inserted without admitting gas to the high-vacuum mass spectrometer chamber. During operation, a small sample of the gas was extracted from the axis of the flow reactor through a 0.3 mm diameter aperture into the first pumped stage of the mass spectrometer system. This was pumped by a 1000 L/s turbomolecular pump (Leybold Turbovac 1000), which was backed by a 40 m^3/h rotary pump (Leybold Trivac D40B). A skimmer cone (0.8 mm diameter) positioned 2.5 cm behind the first aperture was used to form a molecular beam that passed directly into the ionization chamber of the quadrupole mass spectrometer. The ion chamber was pumped by a 70 L/s turbomolecular pump (Varian V70D) backed by a 2.5 m^3/h rotary pump (Balzers Duo 2.5A). The mass spectrometer, operating in direct-current mode, was used to monitor the reactant concentration and any products formed in the heterogeneous reaction. The dual detectors, a

Faraday cup and a channeltron, allowed a wide range of gas concentrations to be monitored simultaneously. The ionizing electron energy (20−150 eV) and current (0.02−2 mA) could be changed to optimize conditions for detection of radical species as well as stable neutrals over a mass range from 0 to 300 amu, but only the standard values of 70 eV and 1 mA were used in this work.

Preparation of Gases. The gaseous HNO_3 reactant was prepared by passing high-purity He through a bubbler containing a 70 wt % solution of nitric acid (Fischer Scientific) held at a temperature of 296 K using a water bath. The flow of the diluted reactant was controlled using a stainless steel fine-metering valve (Nupro, S-series). The mass flow rate was set by observing the change in pressure measured by the Baratron as the gas stream containing reactant was added. The typical procedure of admitting gas to the flow reactor consisted of adding 360 $scm^3\ min^{-1}$ (standard cubic centimeter per minute) He to the reactor using a mass flow controller and throttling the rotary pump until the Baratron read 2.50 mbar. The He mass flow rate was then decreased by an amount equivalent to the desired flow rate of reactant gas stream, typically 5−50 $scm^3\ min^{-1}$ of diluted reactant (which would lead to a HNO_3 concentration of $(3.5-35) \times 10^{12}$ molecules cm^{-3} in the reactor). Finally, the reactant was added until the pressure gauge reading returned to 2.50 mbar.

The reactant gas concentration was calibrated using the vapor pressure data for nitric acid solutions of Brimblecombe and Clegg.[22] The partial vapor pressures of HNO_3 and water above the 70 wt % solution were calculated to be 5.7 and 4.7 mbar, respectively, at 298 K. These values were checked by comparison with the total vapor pressure value of 9 ± 1 mbar measured approximately in this work at 296 K and by measurement of the partial pressure of HNO_3 using UV absorption spectroscopy. The error in the reactant gas concentration was estimated to be 20% due to errors in the concentration of the HNO_3 solution (±2%), the temperature of the water bath (±2 K), and the vapor pressure data. The relatively small amount of water vapor originating from the 70 wt % HNO_3 solution has a negligible effect on the uptake coefficients measured, as will be demonstrated later. This observation is supported by the work of Beichert and Finlayson-Pitts,[18] who found similar uptake coefficents using either anhydrous HNO_3 or a 70% solution as a source of reactant gas.

The water vapor was obtained by evaporation of spectroscopic grade water (Fluka, Hplc grade) held in a 500 mL Pyrex vessel connected to the flow tube via a needle valve. The flow rate was determined using the same method described for HNO_3, by monitoring the change in the reactor pressure when water was added. The temperature of the water sample was controlled by a water bath surrounding the sample. The bath temperature was increased using a heating plate to maintain the required flow rates (up to 1430 $scm^3\ min^{-1}$).

Detection of Reactants and Products. HNO_3 was detected at mass 46 (corresponding to NO_2^+), since the signal was about 2 orders of magnitude higher than that recorded at the parent mass 63. Even when the electron energy and current were lowered to reduce fragmentation of the parent species, the mass 46 peak still dominated. HCl was detected at the parent peak at mass 36.

Under typical operating conditions, the mass spectrometer is easily able to detect changes of gas-phase concentrations of HNO_3 and HCl of the order of 5×10^{10} molecules cm^{-3}, which corresponds to a sensitivity of <1 part in 10^6 for a total pressure of 2.5 mbar in the flow tube. This limited the minimum reactant concentration that could be used for rate measurements in this work to 5×10^{11} molecules cm^{-3}. Under conditions of constant total pressure and flow velocity, a plot of NO_2^+ signal against reactant concentration, determined by the mass flow rate and partial vapor pressure of HNO_3, was linear over the concentration range $(5-500) \times 10^{11}$ molecules cm^{-3}. However, when the reactant concentration and flow velocity were kept constant, but the total pressure was increased, then the reactant signal also increased. This did not affect the results, since the uptake coefficient under given conditions is obtained from the fractional loss of reactant. Measured values of γ were found to be independent (±10%) of total pressures from 0.8 to 5.0 mbar. It was also found that if the total pressure, partial pressure of HNO_3, and the velocity were kept constant, but the relative amounts of He and water vapor were changed, then the reactant signal also changed. The reactant signal decreased as the relative amount of water vapor increased.

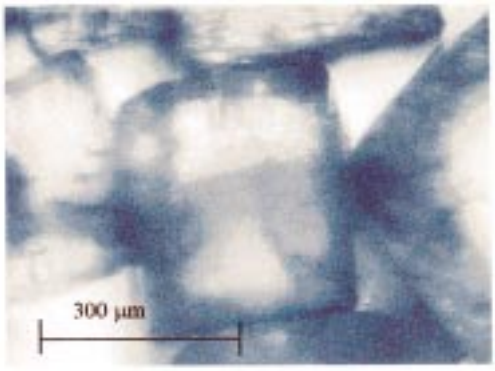

a) Salt grains applied as a single layer to moistened pyrex insert

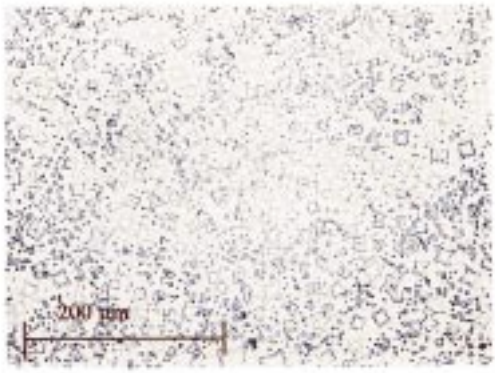

b) Salt crystallites obtained by evaporation of 50%:50% aqueous CH_3OH solution saturated with NaCl

Figure 2. Photomicrograph of NaCl crystallites used for uptake studies.

Preparation of the Reactive Surface. Two distinct types of salt surface were used in this work. The first was made using commercial NaCl grains (Breckland Scientific), diameter of approximately 500 μm, which were used to line the inside of the Pyrex inner tube. The grains adhered to the inner wall to form a layer approximately one grain thick. The physical appearance of this layer is shown in the photomicrograph (Figure 2a), where it can be seen that the grains are fairly close-packed on the Pyrex wall. This thickness was chosen to avoid the

problems associated with diffusion through the internal spaces in the sample when several layers of salt grains are used (Leu et al.[17]). The preparation involved wetting the inside of the Pyrex tube (previously cleaned by soaking in Decon 90 and rinsing with distilled water) with high-purity water. Sieved grains were then poured down the center of the tube, supported vertically, so that they stuck to the water on the walls to form clusters. The grains were then flattened against the inner wall by inserting a solid stainless steel rod, 8 mm o.d. and 1 m in length, and rolling it around the inside of the Pyrex tube. Extra salt grains were added as required via the open ends of the tube and flattened against the inner wall to fill any gaps. The top 10 cm and lower 5 cm of the tube were left uncoated such that the salt grains covered a 60 cm length of tube. In the previous work of Fenter et al.[14,16] and Beichert and Finlayson-Pitts,[18] the uptake coefficient was found to be dependent only on the geometric surface area of the container holding the salt sample and was independent of the number of layers of salt. The total geometric surface area in this work is approximately 250 cm^2 (taking into account the thickness of the salt layer), and the mass of the sample is approximately 27 g. Excess water was removed by drying the surface using a heat gun and also by pumping on the surface after insertion into the flow reactor.

The second type of surface is best described as a dried salt solution. This was prepared by wetting the inside of the inner tube with a saturated solution of NaCl in high-purity water (Fluka, Hplc grade) or methanol (Sigma Aldrich, Hplc grade) or a mixture of the two solvents. Excess salt solution was drained away before inserting the inner tube inside the flow reactor. The salt solution was quickly dried by pumping out the reactor. After the reactor was pumped for just a few seconds, the transparent salt solution was observed to transform to a slightly opaque dry solid. The thickness of the solid layer varied with the relative composition of water and methanol in the saturated solution, owing to the greater solubility of NaCl in water compared with methanol. The relative percentage concentrations of water to methanol, by volume, used in this work were 100:0, 75:25, 50:50, 25:75, and 0:100%. The top 10 cm and lower 5 cm of the surface were not used in this work because of imperfections caused by the preparation technique. The solution may flow down the tube slightly before it has completely dried, leading to gaps at the top of the tube and excess salt at the bottom. These surfaces varied in their visual characteristics, as observed by optical microscopy, and their reactivity, as discussed below. A typical crystallite surface obtained with a 50:50 H_2O/CH_3OH surface is shown in the photomicrograph (Figure 2b).

Calculation of γ Correction Terms and Errors. The rate equation for a heterogeneous reaction in a cylindrical flow tube is given by[23]

$$\frac{-\mathrm{d[X]}}{\mathrm{d}t} = \gamma\frac{\bar{c}}{4}\frac{S}{V}[\mathrm{X}] = k[\mathrm{X}]$$

Integration with respect to time gives

$$\ln[\mathrm{X}] = -k\mathrm{t} + \text{constant}$$

γ is the uptake coefficient, $\bar{c}$ is the average molecular speed, S/V is the surface-to-volume ratio of the reaction vessel ($S/V = 2/r$ for a cylindrical reactor, where r is the radius), and k is the first-order rate constant ($k = \gamma\bar{c}/(2r)$).

The first-order rate constant was measured by monitoring the steady-state reactant concentration over a range of reaction zone lengths l. These lengths are related to the reaction time t by the relationship $t = l/v$, where v is the average flow velocity of the gas. k was calculated from the gradient of a plot of ln-$[HNO_3]$ against reaction time, and the uptake coefficient γ was derived from the equation

$$\gamma = 2r\frac{k}{\bar{c}} \qquad \text{(i)}$$

Corrections for γ need to be considered for the typical laminar flow conditions used in this work. The axial pressure gradient along the flow reactor was calculated to be 0.02 mbar and considered to be negligible. The correction for axial diffusion was also calculated and found to be insignificant (<1%).

The correction for radial diffusion was made using the methods described by Brown.[24] In He carrier gas the magnitude of the correction was small (<25%) for the relatively unreactive surface in these experiments ($\gamma < 1 \times 10^{-3}$). However, in the experiments using high water vapor pressures, the correction term was much larger because of the higher total pressures used and the slower diffusion of HNO_3 in water, which was estimated to be $D = 0.124$ atm cm^2 s^{-1} at 298 K (obtained by analogy with diffusion coefficients for SO_2 (Van Doren et al.[25])) compared with HNO_3 in He ($D = 0.534$ atm cm^2 s^{-1}). The correction term due to radial diffusion ranged from ~15% at 1 mbar of H_2O to a factor of >2 at 10 mbar of H_2O.

Uncertainties in the absolute values of γ are expected to be reasonably large because of the limited repeatability of the preparation of the salt surface. However, upon comparison of γ values measured on seven different salt grain surfaces under similar experimental conditions (fresh and dried, no added water vapor, $[HNO_3] = 6 \times 10^{12}$ molecules cm^{-3}), the standard deviation was found to be $\pm 4 \times 10^{-5}$ for a mean γ value of 2.3×10^{-4}. An error of ±20% is assigned for this.

To reduce such errors, the same surface was used for all measurements in which a specific trend was investigated (e.g., the effect of $[HNO_3]$ on γ for dry salt grains). The error associated with such a series of measurements is estimated to be ±20% and is due to baseline drift and noise in the mass spectrometric signal, flow and pressue fluctuations, etc.

A further error needs to be considered to account for changes in γ due to the continuous decline in reactivity of the salt surface with HNO_3. In certain cases, it has been possible to apply small correction factors to adjust the γ values measured on a partially saturated surface so that they are consistent with those calculated on the original fresh surface. These corrections allow γ values to be compared over the whole range of conditions used in this work. An error of approximately ±25% accounts for saturation effects. Hence, the total error in γ is less than ±37%. This does not take into account errors associated with the assumption that the geometric surface area represents the actual surface area available for reactive uptake. Irregularities in the surface would lead to a larger surface area, as discussed by Keyser et al.[26] and hence an overestimate of the uptake coefficients calculated by eq i.

3. Results

3.1. Salt Grain Surfaces. *Initial Uptake.* Figure 3 illustrates the uptake of HNO_3 and production of HCl on dried salt grain surface. The initial reaction rate upon exposure of a freshly prepared and dried salt grain surface to gaseous HNO_3 is rapid but is time-dependent, the rate of reaction decreasing to a steady-state value after approximately 15 min. This behavior has been reported previously by all three groups studying the uptake kinetics of HNO_3 on NaCl.[14−18] Beichert and Finlayson-Pitts[18] proposed that the high initial uptake rate

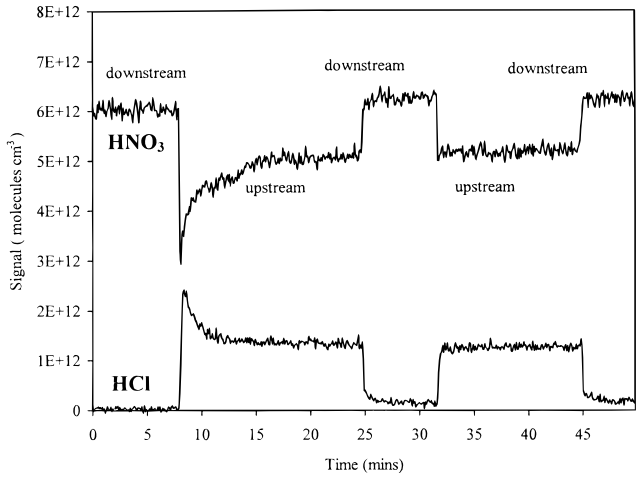

Figure 3. Uptake of HNO_3 and production of HCl on dried salt grain surface: $[HNO_3]$ = molecule cm^{-3}; $p(H_2O) \approx 0.001$ mbar; total pressure = 2.25 mbar.

is due to the presence of adsorbed water on the surface, which cannot be removed by extensive pumping of heating of the salt grains. All values for the uptake coefficient, γ, reported in this work on salt grains have been measured under steady-state conditions only. Figure 3 also shows that the amount of HCl produced in the reaction is equal to the amount of HNO_3 that is taken up by the salt. This shows that only reactive uptake is being measured, as opposed to physical adsorption, and that HCl is the only gaseous product of the reaction. A search for other possible reaction products, Cl_2 and HOCl, was made at appropriate mass numbers, but none were found.

Kinetics of HNO_3 Decay. The uptake coefficient, γ, was calculated using eq i, assuming that the decay of HNO_3 along the coated section of the flow tube follows first-order kinetics. To test this, the HNO_3 concentration was measured as a function of reaction zone length *l*. Figure 4 shows mass spectrometer signals at masses 46 and 36, corresponding to HNO_3 and HCl, obtained when the zone length was changed in steps of 20 cm every 100 s for both increasing and decreasing length *l*. The changes in the signals when length *l* was changed were simultaneous within the time resolution of the measurements (5 s). Also, the magnitudes of the concentration changes of HNO_3 and HCl were equal.

A plot of $\ln[HNO_3]$ against *l* is shown in Figure 5. It can be seen that $\ln[HNO_3]$ at a particular point is constant, irrespective of whether length *l* has been increased or decreased; i.e., $\ln[HNO_3]$ at a given length *l* is independent of the history of the surface, on the time scale of these measurements. The decay of $\ln[HNO_3]$ is linear, as expected for a first-order reaction. However, the fractional decay of HNO_3 in this experiment was only 15%, so this does not provide a stringent test for decay kinetics. Nevertheless, the first-order rate equation was assumed to be valid for the small fractional decays employed for the rate measurements and the determination of the corresponding γ values. Wherever possible the psuedo-first-order rate coefficient was determined by measuring the steady-state $[HNO_3]$ at 0, 20, 40, and 60 cm. However, to conserve surface reactivity during experiments where the effects of $[HNO_3]$ and $[H_2O]$ variation were investigated, only measurements at 0 and 60 cm were used.

Effect of $[HNO_3]$ on γ. To provide a further test of the kinetic order of the reaction, the uptake coefficient determined from the pseudo-first-order rate constants was measured over a wide range of initial $[HNO_3]$ from 6×10^{11} to 7×10^{13} molecules cm^{-3}. These data are presented in Figure 6, which shows a

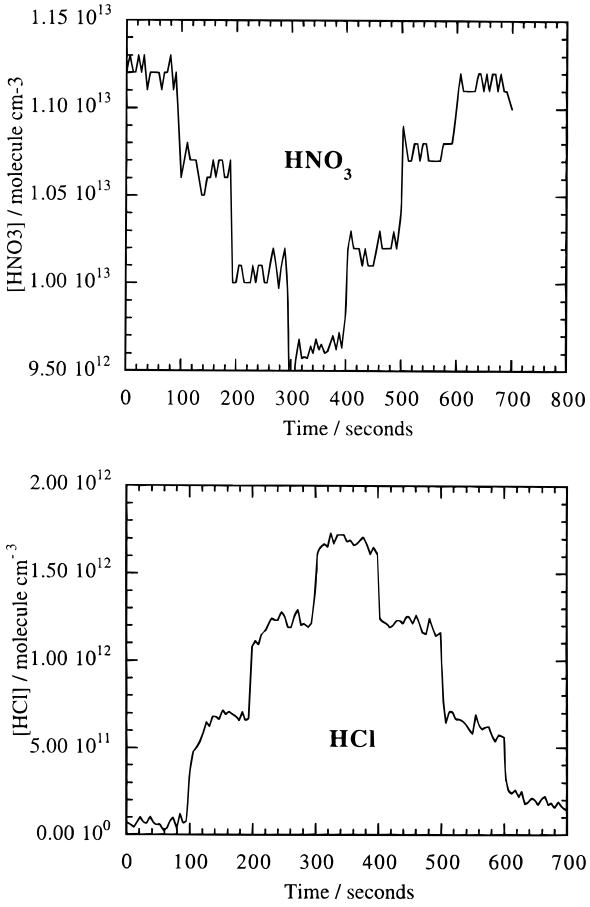

Figure 4. Mass spectrometer signals at masses 46 and 36 (HNO_3 and HCl respectively) as a function of zone length. Flow velocity = 1700 cm s^{-1}.

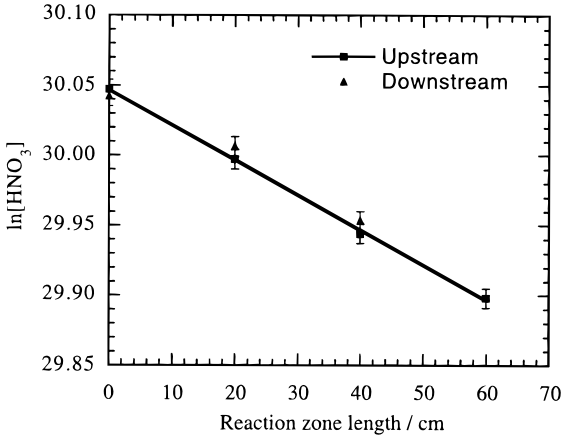

Figure 5. Plot of $\ln[HNO_3]$ against zone length *l* for data shown in Figure 4, showing upstream data from increasing zone length and downstream data from decreasing zone length.

logarithmic plot of γ vs $[HNO_3]$. γ decreased as $[HNO_3]$ increased, the dependence being well described by a power relationship

$$\gamma \approx [HNO_3]^{-(0.5\pm0.1)}$$

The relationship was observed irrespective of whether measurements were made with increasing or decreasing $[HNO_3]$, showing that the effect was not due to permanent saturation or declining reactivity of the surface.

Effect of $[H_2O]$ on γ. The effect of a variation in water vapor partial pressure in the range 0.0002 to 10 mbar on the uptake

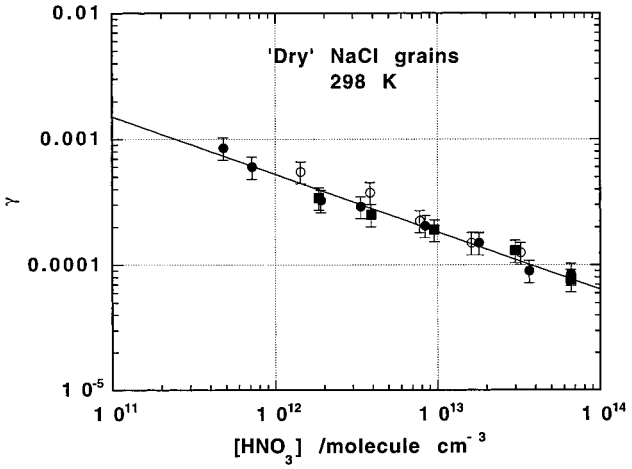

Figure 6. Plot of $[HNO_3]$ dependence of the uptake coefficent γ. Filled points show data obtained by successive reduction in $[HNO_3]$. Open points are results associated with increasing $[HNO_3]$.

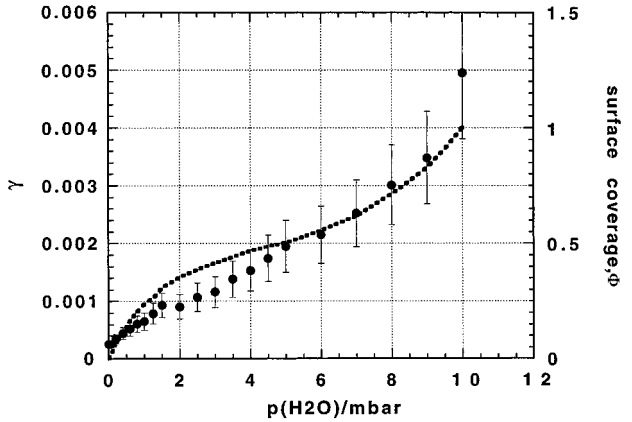

Figure 7. Water vapor dependence of γ: $[HNO_3] = (6.0 \pm 1.0) \times 10^{12}$ molecule cm^{-3}; total pressure of 5 mbar for $p(H_2O) \leq 5$ mbar and total pressure of 10 mbar for $p(H_2O) \leq 10$ mbar. Broken line shows isotherm for H_2O adsorption, expressed as surface coverage, on polycrystalline NaCl, reported by Barraclough and Hall.[21]

coefficient was investigated using a fixed $[HNO_3]$ of 6×10^{12} molecules cm^{-3} and a fixed flow velocity of 17 m s^{-1}. The lower limit of $p(H_2O)$ was determined by the water present in the HNO_3 flow and the upper limit by constraints in the practical operation of the flow tube. In the first series of experiments, the total pressure was kept constant at 5 mbar and the He was progressively replaced by H_2O. Helium was then added to give 10 mbar and again progressively replaced by H_2O. The corrections made to the rate data for radial diffusion amounted to an upward correction of a factor of >2 at the highest water vapor pressures.

The data are shown in Figure 7 where it will be seen that γ increased steadily from its "dry salt" value throughout the range investigated. Also shown in Figure 7 is an isotherm at 298 K for water adsorption on polycrystalline NaCl, obtained by Barraclough and Hall.[21] The maximum $p(H_2O)$ used here (10 mbar) corresponds approximately to the first inflection point on the adsorption isotherm for water on polycrystalline NaCl obtained by these and other workers.[19,20] This is well below the deliquescence point for NaCl at ambient temperature (~25 mbar of H_2O), but the indications from the water adsorption isotherms on NaCl point strongly to amounts of adsorbed water up to and exceeding one monolayer equivalent in this regime. The similarity of the H_2O dependence of γ to the water isotherm suggests that reactive uptake rate depends on the volume of adsorbed water.

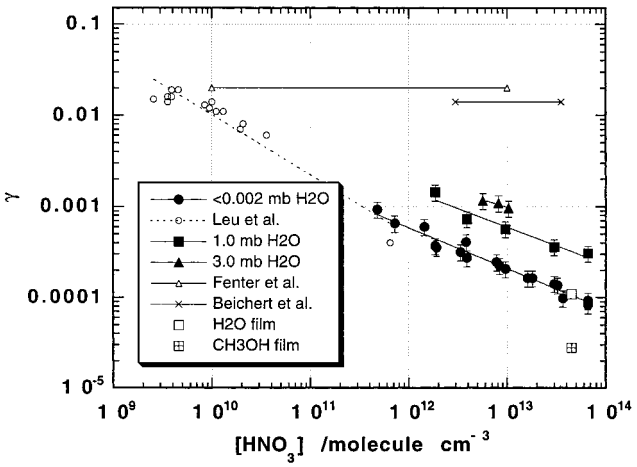

Figure 8. Effect of initial $[HNO_3]$ on the uptake coefficient at 298 ± 3 K. Data are from present work: (●) <0.004 mbar H_2O; (■) 1.0 mbar H_2O; (▲) 3.0 mbar H_2O; (○) Leu et al;[17] (△) Fenter et al.;[16] (×) Beichert and Finlayson-Pitts.[18] The data shown summarizes results from the present study and those of others using dry salt grains. Data for dried salt film obtained in this study also shown.

The effect of initial $[HNO_3]$ was investigated at several water vapor concentrations. The data are shown in Figure 8, which summarizes results from the present study and those of others using dry salt grains. Data obtained with 1 mbar of H_2O in which HNO_3 was varied by a factor of 47 show a power relationship similar to that observed for "dry salt". A smaller range of HNO_3 was used at higher $p(H_2O)$, but the resulting changes in γ were consistent with the power dependence observed at lower $p(H_2O)$. A similar relationship between γ and $[HNO_3]$ is indicated in the data of Leu et al.,[17] although they chose to report a single value for γ averaged from their data obtained at much lower $[HNO_3]$ than in the present work. Discussion of the other data shown in Figure 8 is deferred to the discussion section.

Other Uptake Measurements. The uptake of HCl on the surface of NaCl, which had previously been reacted with HNO_3, was investigated. The initial concentration of 6×10^{12} molecule cm^{-3} HCl decreased on exposure to the surface, and this was accompanied by the appearance of a signal at mass 46 corresponding to an equivalent production of HNO_3. This indicates that the overall reaction of HNO_3 on NaCl is reversible. However, no evolution of HNO_3 occurred when gaseous HCl was exposed to a surface of $NaNO_3$ grains prepared in a way similar to that for NaCl. A temporary drop in [HCl] (initially 6×10^{12} molecule cm^{-3}) was observed on exposure, showing that HCl is physically adsorbed on this surface. Exposure of HNO_3 to the $NaNO_3$ surface also resulted in a temporary drop in concentration that recovered after several minutes. On return of the injector to the original position, a temporary increase in $[HNO_3]$ was observed, showing that adsorption was reversible.

3.2. Dried Salt Solution Surfaces. Reactive uptake of HNO_3 was also investigated on the films of dried salt deposited on the walls of the flow tube. When the surface film of NaCl was first exposed to HNO_3, reactive uptake was observed with corresponding production of HCl. The uptake rate at a given injector position remained approximately constant for a few minutes or longer, depending on the $[HNO_3]$. The uptake rate started to decline after approximately 10^{15} HNO_3 molecules per cm^2 had reacted, corresponding to reaction of approximately 1 monolayer of surface atoms. Thereafter, the reaction rate fell off steadily to zero. Clearly, the reactivity of the dried salt films became saturated much more quickly than the salt grain surfaces

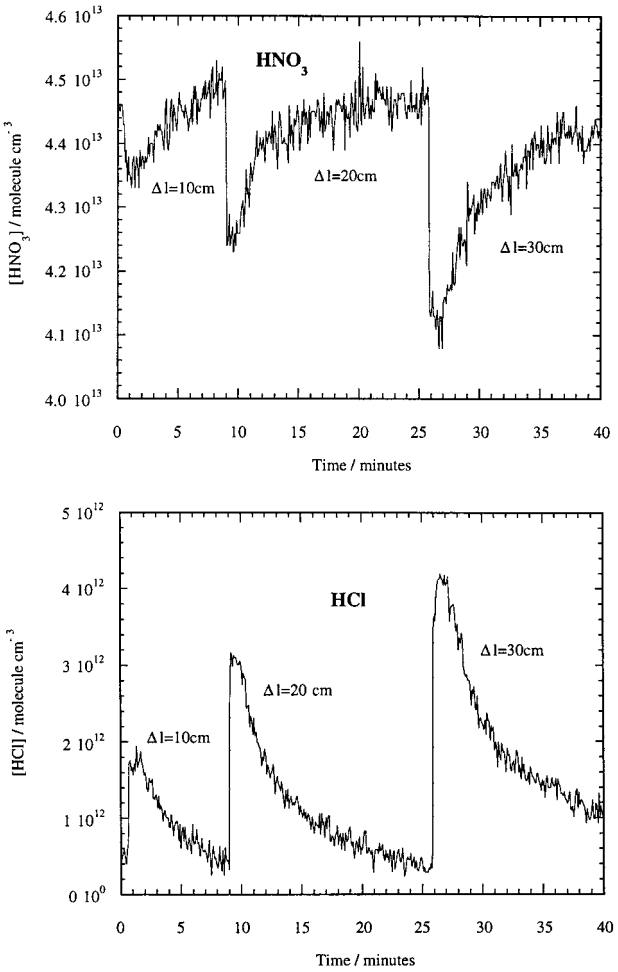

Figure 9. Reactive uptake of HNO_3 investigated on the films of dried salt deposited on the walls of the flow tube from aqueous solution. $[HNO_3] = 4.5 \times 10^{12}$ molecule cm^{-3}.

such that γ could not be easily measured under steady-state conditions in the conventional way in our system. However, the initial time-independent signal was reproducible for similar fresh salt samples and was therefore used to make kinetic measurements. Since any part of the salt surface exposed to HNO_3 could only be used once (due to saturation), the kinetic information was obtained by exposing only the first 10 cm of the surface to HNO_3, measuring the time-dependent uptake and then waiting for the surface to become saturated. This procedure was repeated for the next 20 cm of the surface and then for the remaining 30 cm such that all 60 cm of the surface had become saturated as shown in Figure 8. Kinetics data were obtained from a plot of ln[HNO_3] (measured before saturation) against reaction zone length, and γ was calculated using eq i. For the conditions illustrated in Figure 9([HNO_3] = 4.5×10^{13} molecule cm^{-3}), the value obtained was $\gamma = 1.1 \times 10^{-4}$, which is in good agreement with the result for dry salt grains at the same [HNO_3] (see Figure 8). Thus, the surface reaction rate of the salt samples is similar. The lower capacity for reaction of the salt film appears to be due to the smaller mass of the salt sample available for reaction, the mass of the film being about a factor of 100 lower than the mass of the grains. The physical explanation of this effect is not obvious.

The uptake coefficient was also measured on dried salt surfaces made from saturated solutions containing varying compositions of water and methanol. Both the thickness of the film and the amount of surface adsorbed water are expected to decrease as methanol replaced water as solvent. A high [HNO_3]-($\sim 4.5 \times 10^{13}$ molecule cm^{-3}) was used to shorten the data collection time required to saturate the surface. The results are shown in Table 1 for saturated NaCl solutions made with 0, 25, 50, 75, and 100% water by volume, the balance being methanol. Clearly, γ decreases as the amount of water in the solution decreases, the change being approximately a factor of 4 between pure water and pure methanol. Since the initial γ on a fresh surface is not affected by the mass of the salt sample and since on inspection with a microscope there was no visual evidence to suggest that the surface area of the films was vastly different, these results suggest that the reactivity is affected by the amount of water present in the "dry" salt films.

TABLE 1: Uptake Coefficients on Dried Salt Films

CH_3OH %	[HNO_3] molecule $cm^{-3} \times 10^{13}$	$\gamma \times 10^{-5}$
0	4.5	11.0
25	4.7	9.1
50	4.0	6.5
75	4.4	4.0
100	4.5	2.8

4. Discussion

Comparison with Previous Work. Figure 8 shows values of γ obtained in this work and in earlier work plotted against the HNO_3 concentration. The claimed overall uncertainty in the reported values of γ is approximately a factor of ± 2 in each case. The most noticeable feature is that the values of the steady-state reactive uptake coefficient measured in the present work, both on grains and thin film deposits of NaCl, are much lower than reported previously for dried NaCl, except for the measurements of Laux et al.,[15] using a single crystal of NaCl ($\gamma \approx 5.0 \times 10^{-4}$). The other feature of the present work is the falloff in γ with increasing HNO_3 concentration. Although saturation effects resulting from exposure of salt samples to HNO_3 have been reported in all studies, a systematic dependence of the steady-state uptake coefficient on [HNO_3] has not been reported previously. In the present work we took care to try to account for surface exposure history in the measurement protocols, and we believe that the concentration effect is a real feature of the uptake kinetics.

Extrapolation from the present data to the much lower [HNO_3] regime employed by Leu et al.[17] shows reasonable consistency in the γ values for dry salt when the factor of 2 uncertainty in the absolute values of γ is taken into account. However, this comparison may not be valid, since the Leu et al. data were "corrected" for pore diffusion, the measured reaction rates being a factor of 2−4 higher. The uptake coefficients measured under Knudsen cell conditions[14,16,18] agree well with each other, but neither shows any [HNO_3] dependence over a large range. Although they agree well with the "corrected" γ values obtained by Leu et al.[17] at low [HNO_3], the values at comparable [HNO_3] are a factor of 10−100 times larger than those measured in the present study.

Leu et al.[17] made substantial corrections to their uptake data to account for the effect of in-pore diffusion of the reactant gas into the bed of salt grains, which provided the reactive surface in the flow tube. Fenter et al.[16] successfully used this diffusion model to explain the sample depth dependence they observed for the reactive uptake of N_2O_5 on NaCl powders, but for reactive uptake of HNO_3 they observed no such dependence on sample presentation, the uptake rate being apparently determined by the geometric surface area. This was explained in terms of strong, reversible, physical uptake of HNO_3 on the NaCl surfaces, which effectively prevented diffusion of HNO_3

into the internal surfaces of the salt sample. Beichert and Finlayson-Pitts[18] also observed uptake rates that were dependent only on the geometric surface area and were independent of particle size or the depth of the sample. They suggest that the structure of the solid sample in the Knudsen reactor does not have deep pores accessible to the gas, so only the external surface is active. They point out that the "adsorption" hypothesis of Fenter et al.[16] would also apply to the studies of Leu et al.,[17] making the downward correction of the uptake rates invalid, resulting in γ values approximately a factor of 2−4 higher than those measured in the Knudsen cell studies.

Most of the uptake measurements of Fenter et al.[14] were made under "low-dose" conditions, where saturation effects were not observable. They observed significant induction periods for HCl production, and they also found reversible uptake with almost identical uptake probability for HNO_3 on NaCl, KCl, and $NaNO_3$ and for HCl on NaCl. This suggests strongly that the measured rates apply to nonreactive uptake, possibly the reversible process proposed to explain the apparent absence of pore diffusion. In any case it is clear that γ values derived from these measurements are not directly comparable to the steady-state reactive uptake rates measured in the present study. The γ values reported by Fenter et al.[16] at low doses probably represent uptake rates for physical adsorption of HNO_3, which may be reversible; an adsorbed precursor species may then react to form HCl, which is eventually desorbed. Their proposed multistep model for the surface reaction of HNO_3 on salt describes this sequence.

The Knudsen cell results of Beichert and Finlayson-Pitts[18] were obtained under conditions of steady-state reactive uptake similar to the conditions in the present study, in which the initial, time-dependent rapid uptake of HNO_3 had reached saturation but before the chemical reactivity of the surface had been exhausted. They used a shallow layer of 500 μm salt grains and used the geometric surface area to calculate γ. We are unable to account for the difference of a factor of 100 between the kinetic results from the two studies; it probably refects the different salt surfaces and their degree of deactivation resulting from exposure to HNO_3.

Mechanism of the Reaction of Gaseous HNO_3 with NaCl (s). The experimental observations for HNO_3 reaction with solid salt are consistent with the reaction occurring in three stages: (1) adsorption of gaseous HNO_3 molecules at favorable surface sites; (2) reaction at these surface sites with Cl^- ions to form HCl molecules; (3) desorption of HCl molecules to the gas phase. There is compelling evidence from the H and D isotope studies of Beichert and Finlayson-Pitts[18] that surface adsorbed water molecules are intricately involved in the surface reaction. They suggested that strongly adsorbed water molecules, which are present even on vacuum-dried NaCl samples where they occupy defect sites on the surface of the crystals, are able to efficiently promote the reaction. The importance of defect sites is emphasized by the much reduced rate of reaction when single-crystal surfaces are exposed to HNO_3 vapor.[15] The observations in the present work show that the reaction rate increases with gas-phase pressure of H_2O in the region where studies of water adsorption on NaCl surfaces indicate increasing coverage of H_2O molecules. This suggests that more defect sites become reactive as the water vapor pressure increases.

The participation of water in the reaction suggests that ions produced by solvation of HNO_3 molecules adsorbed at the surface are involved. We propose that this occurs by a two-step process: adsorption of HNO_3 molecules on the surface followed by their diffusion to defect sites where water molecules

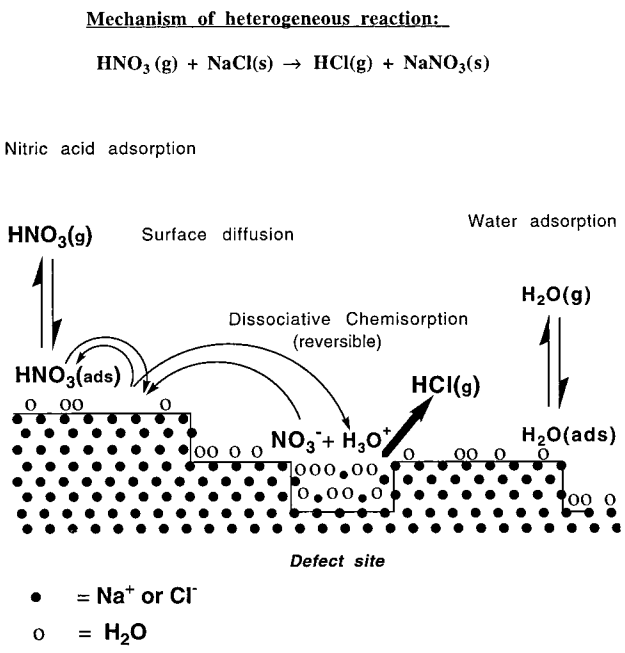

Figure 10. Schematic diagram illustrating proposed mechanism for the HNO_3 + NaCl heterogeneous reaction.

are adsorbed, as illustrated in Figure 10. Here, dissociation occurs with formation of adsorbed hydronium ions and nitrate ions. The overall process is assumed to be reversible:

$$HNO_3\,(g) \leftrightarrow HNO_3\,(ads) \overset{H_2O}{\leftrightarrow} H_3O^+\,(s) + NO_3^-\,(s)$$

The occurrence of reversible adsorption of HNO_3 on the surface of NaCl crystals as a process distinct from the reaction at the surface forming HCl is demonstrated clearly by the observations by both Fenter et al.[14] and Leu et al.[17] At low doses such that surface saturation effects were resolvable, Fenter et al.[14] observed rapid uptake of HNO_3 but a delay in the release of HCl. At room-temperature Leu et al. observed uptake of HNO_3 with prompt HCl production, while at low temperature (227 K), rapid initial uptake occurred with a low yield of HCl. The uptake saturated after a few minutes, and HCl production was initially only 5−10% of the HNO_3 adsorbed and subsequently dropped to zero. When the HNO_3 flow was stopped, 90−95% of the HNO_3 was desorbed, showing that predominantly reversible adsorption had occurred without chemical reaction of HNO_3.

Following Beichert and Finlayson-Pitts,[18] we propose that formation of HCl molecules occurs via a surface reaction of adsorbed H_3O^+ with chloride ions present in a layer of adsorbed water at surface defects:

$$H_3O^+ + Cl^- \leftrightarrow HCl\,(ads) \rightarrow HCl\,(g)$$

Solid $NaNO_3$ forms on the surface at the same time. HCl molecules are expected to rapidly desorb from the surface, since uptake and physical adsorption of HCl gas on both NaCl and $NaNO_3$ surfaces appear to be weak.[14,18]

Barraclough and Hall[21] have reported an extensive study of the adsorption isotherms for H_2O on polycrystalline alkali halides, including NaCl. Only after adsorption of the first two monolayer equivalents ($p(H_2O)$ = 15 mbar at 298 K) did the system behave as if a saturated solution of NaCl was present. The experimental observations at lower coverages, i.e., the stepwise nature of the isotherm, were attributed to two-

dimensional condensation. Recent studies carried out using well-defined NaCl surfaces (clean 100 faces) exposed to water vapor[27,28] also point to formation of a two-dimensional condensed phase at submonolayer surface coverages. However, three-dimensional condensation is likely to occur at some defect sites where water molecules are strongly bound.

The studies all show that following the reactive event, at least some of the defect sites are regenerated and can sustain further HNO_3 adsorption and reaction with Cl^-. Laux et al.[29] suggest that this occurs as a result of surface migration of NO_3^-, leaving new Cl^- exposed. They observed recrystallized satellite $NaNO_3$ structures following reaction of HNO_3 with NaCl crystals followed by exposure to water. On the other hand, Peters and Ewing[30] suggest that NO_3^- formed by reaction of N_2O_4 with NaCl forms a 2-D layer structure of $NaNO_3$ on the surface, which causes dislocation of the underlying NaCl structure, leaving new defect sites with exposed Cl^-. Timonen et al.[31] have suggested the same process for the $ClNO_3$ + NaCl reaction. Whatever the mechanism, it is clear that under the conditions of steady-state reaction, Cl^- ions from the inner layers of the salt matrix become available to sustain reactivity on the surface.

HNO_3 Dependence of the Steady-State Uptake Coefficient. Beichert and Finlayson-Pitts[18] have rationalized the rate-controlling processes occurring in the surface adsorbed water in terms of bulk aqueous thermodynamic parameters of the ionic species involved. However, we prefer a description of the kinetics in terms of a surface reaction. According to this model, the rate of HCl formation (molecule cm^{-3} s^{-1}) is given by

$$\frac{d[HCl]}{dt} = k_r N_s \theta_N \frac{S}{V}$$

where N_s is the number of defect sites per unit area available for reaction (i.e., with available Cl^-), k_r is a rate coefficient for surface reaction, θ_N the fraction of the defect sites with H_3O^+ present because of reversible adsorption of HNO_3, and S/V is the surface/volume ratio. Under conditions of steady-state uptake N_s remains constant because of regeneration.

The HCl formation rate may be equated with the net loss of HNO_3 from the gas phase, which is given by

$$\frac{-d[HNO_3]}{dt} = k^I[HNO_3] = \frac{\gamma \bar{c}}{4}[HNO_3]\frac{S}{V}$$

leading to the following expression for the uptake coefficient:

$$\gamma = \frac{4k_r N_s}{\bar{c}} \frac{\theta_N}{[HNO_3]} \qquad \text{(ii)}$$

An expression for the surface coverage term for HNO_3, θ_N, can be derived using an appropriate adsorption model. We assume that the primary adsorptive process driving loss of gas-phase HNO_3 is dissociative chemisorption; i.e., interaction of physisorbed HNO_3 with surface-phase water occurs with production H_3^+O and NO_3^- on adjacent sites. It is further assumed that the rate of reaction with Cl^- is slow compared with associative desorption (this may be the case for steady-state reaction when substantial $NaNO_3$ is already formed on the surface). In the case of the Langmuir model for dissociative adsorption (ref 33, p 889), the rate of adsorption is proportional to the gas concentration and the probability that both species will find sites ($=[HNO_3]\{N_s(1-\theta_N\}^2$). The rate of desorption is proportional to the frequency of encounters of the surface adsorbed species and is proportional to $\{N_s\theta_N\}^2$. Equating these rates gives the following expression for the surface coverage in terms of the gas-phase concentration:

$$\theta_N = \frac{(K_e[HNO_3])^{1/2}}{1 + (K_e[HNO_3])^{1/2}} \qquad \text{(iii)}$$

where K_e is the equilibrium constant for reversible dissociative chemisorption of HNO_3 on the surface. If it is assumed that only a small fraction of the sites are occupied, i.e., $(K_e[HNO_3])^{1/2} \ll 1$, we obtain the following functional dependence of γ on $[HNO_3]$:

$$\frac{1}{\gamma} = \frac{\bar{c}}{4k_r N_s K_e^{1/2}}[HNO_3]^{1/2} \qquad \text{(iv)}$$

Therefore, a plot of $1/\gamma$ vs $[HNO_3]^{1/2}$ should be linear and should pass through the origin. Data for the $[HNO_3]$ dependence of γ are plotted in this form in Figure 11 for experiments with no added water and with $p(H_2O)$ = 1 and 3 mbar.

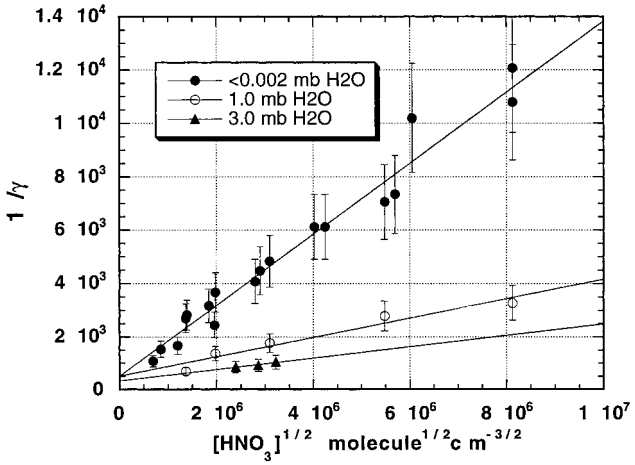

Figure 11. Plot of $1/\gamma$ vs $[HNO_3]^{1/2}$ for data using 0, 1.0, and 3.0 mbar of added H_2O vapor.

TABLE 2: Analysis of HNO_3 Dependence of γ

added $p(H_2O)^a$	slope[b]	intercept	$k_r N_s (K_e)^{1/2}$ [c]
0	13.3 ± 1.2	520 ± 506	5.45
1.0	3.6 ± 1.0	515 ± 480	19.8
3.0	2.1 ± 1.4	333 ± 388	37.6

[a] In mbarr. [b] In $cm^{3/2}$ $molecule^{-1/2} \times 10^4$. Standard deviation = $\pm 2\sigma$. [c] In $cm^{-1/2}$ $molecule^{1/2}$ $s^{-1} \times 10^{-6}$.

Both data sets, which have a wide range of $[HNO_3]$, give approximately linear plots, the slope decreasing with added water. There appears to be a significant positive intercept, indicating that the model assumptions are not fully valid. The slopes and intercepts for data at 0, 1, and 3 mbar H_2O are summarized in Table 2, together with the quantity $k_s N_s (K_e)^{1/2}$ calculated from the slope.

The assumption that $K_e[HNO_3])^{1/2} \ll 1$ requires a Langmuir constant for HNO_3 adsorption of 10^{-16} cm^3 $molecule^{-1}$ for the highest $[HNO_3]$ used in the present work. According to a simple kinetic model of Adamson[32] for adsorption/desorption,

$$K_e = \sigma\tau_0(2\pi mkT)^{-1/2} \exp(-\Delta H^\circ_{ads}/RT) \qquad \text{(v)}$$

where σ is the molecular diameter and τ_0 is the vibrational frequency of the surface−adsorbate bond ($\sim 10^{-13}$ s^{-1}). By use of $\sigma = 0.6 \times 10^{-18}$ m^2, the above upper limit for K_e is satisfied if the enthalpy of dissociative adsorption of HNO_3 on NaCl

crystals is -42 kJ mol^{-1}. This is less than the value of $\Delta H = -72.4$ kJ mol^{-1} for the overall reaction $HNO_3(g) \rightarrow H^+(aq) + NO_3^-(aq)$,[32] but greater than the enthalpy of evaporation of HNO_3 (l), -38 kJ mol^{-1}.[33] Considering that adsorption enthalpies at moderate surface coverage are less than the values for the bulk phase changes, a Langmuir constant for HNO_3 adsorption of 10^{-16} cm^3 molecule^{-1} is not unrealistic. Moreover, under conditions of steady-state reactive uptake, product NO_3^- will be present at the reactive sites, tending to inhibit the HNO_3 adsorption equilibrium. The more rapid uptake on fresh NaCl may reflect a larger value of the effective K_e.

Water Vapor Dependence of the Steady-State Uptake Coefficient. Water vapor enhances the reactivity of the surface. We assume that this is caused by adsorbed water increasing the *number* of sites where water adsorption allows Cl^- to be released from the lattice and dissociation of HNO_3 to occur, i.e., increasing N_s. For constant low [HNO_3], eq ii can be written as

$$\gamma = \omega N_s$$

where

$$\omega = \frac{4k_s K_e^{1/2}}{\bar{c}[HNO_3]^{1/2}}$$

The total number of sites S, i.e., Na^+Cl^- ion pairs on a 100 sodium chloride crystal face, is 6.4×10^{14} cm^{-2}. Not all these sites support H_2O adsorption at low relative humidity. The work of Barraclough and Hall[21] shows that with respect to H_2O adsorption, ~25% of the surface of NaCl is composed of "active sites", which are identified with surface impurities, surface defects and hollows. or non-100 planes including corners and edges. Dai et al.[26] showed that ~20% of the surface sites on NaCl crystallites are defects, some of which are chemically reactive with water itself.

Let us assume that the number of reactive sites active at a given partial pressure of H_2O is proportional to the *volume* of adsorbed water V. The number of reactive sites can be expressed as follows:

$$N_s = Sf\frac{V}{V_m}$$

where $f = 0.25$, $S = 6.4 \times 10^{14}$ cm^{-2}, and V_m the volume corresponding to a surface coverage of water $\Phi = 1$. The water isotherm on NaCl exhibits characteristics of multilayer adsorption at $p(H_2O) \approx 10$ mbar (i.e., $V/V_m > 1$). Therefore, a given defect site may support more than one Cl^- reactant, and the surface reactant concentration N_s can be greater than the number of defect sites. The simplest form of isotherm for multilayer adsorption is the BET isotherm, and we have expressed the H_2O dependence of γ according to the equation[33]

$$\frac{z}{(1-z)}\frac{1}{\gamma} = \frac{1}{\gamma_m C} + \frac{(C-1)z}{\gamma_m C} \qquad \text{(vi)}$$

where $z = p/p_0$ (p_0 is the vapor pressure of H_2O at 298 K) and γ replaces V in the BET equation. Figure 11 shows a plot of the data obtained at [HNO_3] $= 6.0 \times 10^{12}$ molecule cm^{-3} according to eq vi. The value of γ obtained without added water vapor was subtracted from the observed values to account for the reactivity of "dry" salt. A generally linear trend is apparent over the range with a slope and intercept values of 232 ± 29 and 86 ± 4, respectively. The corresponding values of $C = 3.7 \pm 0.36$ and $\gamma_m = (3.14 \pm 0.34) \times 10^{-3}$ are obtained. Here, γ_m is the uptake coefficient corresponding to a water surface coverage equivalent to one monolayer. The corresponding value of $p(H_2O)$ at 297 K is 9.9 mbar.

TABLE 3: Number of Active Sites for HNO_3 + NaCl Reaction

added $p(H_2O)$ mbar	N_s cm$^{-2} \times 10^{13}$	total sites %
0	1.6 ± 0.5	2.5
1.0	5.8 ± 1.7	9.0
3.0	10 ± 7	16

According to the model $\gamma_m = \omega f S$, allowing evaluation of $\omega = (1.94 \pm 0.44) \times 10^{-17}$ cm$^{-1/2}$ molecule$^{1/2}$ s^{-1} from the slope and intercept from Figure 11. Since [HNO_3] $= 6.0 \times 10^{12}$ molecule cm^{-3}, we obtain a value for the quantity $k_r K_e^{1/2} = (3.7 \pm 0.8) \times 10^{-7}$ cm$^{-3/2}$ molecule$^{-1/2}$ s^{-1}. The slope of the plots of eq iv gave values for $k_r N_s K_e^{1/2}$, and hence, we can estimate N_s, the number of "active" sites as a function of water vapor concentration at low coverage. Table 3 shows a summary of the values.

The initial rapid rate of uptake of HNO_3, before steady state is established, must be due to reaction on active sites that are present on freshly exposed NaCl, but which are not regenerated. A possible explanation is that NO_3^- formed at these sites inhibits the uptake of HNO_3 and hence reduces the [H_3O^+] or reduces the surface concentration of Cl^-, leading to the initial, time-dependent uptake coefficient.

Reaction of HNO_3 with Sea Salt in the Marine Boundary Layer. The parametrization of the reactive uptake coefficient for the HNO_3 (g) + NaCl (s) reaction in terms of the concentration of HNO_3 and water vapor (eqs iv and vi) can be used to evaluate the uptake coefficient for reaction on sea salt particles. The particulate material produced from the sea can exist as seawater drops, brine drops, or solid salt particles.[5] In the marine boundary layer, relative humidity is normally ~75%, i.e., close to the deliquescent point for NaCl, above which the particles are liquid drops. Below the deliquescent point the supersaturated liquid drops persist until the effluorescence point is reached (37% relative humidity for NaCl), when solid crystalline particles form. On rehumidifying, the particles remain solid up to the deliquescent point, but throughout this regime of intermediate humidity, multilayer adsorption of water produces a quasi liquid water layer and the atmospheric gases will be in contact with saturated brine solution. Although HNO_3 uptake into such solutions is likely to be rapid, gaseous HCl will not be released until the pH falls below 3. The point where this occurs will depend on the amount of adsorbed water and hence on the humidity. The parametrization from the present study was obtained for uptake on solid NaCl with relative humidity up to 35%, corresponding to water adsorption equivalent to approximately one monolayer. At higher relative humidity, multilayer adsorption occurs even on planar 100 surfaces of NaCl, as shown recently in the measurements of Peters and Ewing,[34] which means that the parametrization in eq vi will underestimate γ. However, the HNO_3 dependence according to eq iv will lead to an overestimation of γ, since the experimental data show a positive deviation of $^1/_\gamma$ at low [HNO_3]. These effects may compensate, and uptake coefficients calculated from this parametrization could represent a reasonable estimate of the reaction rate under atmospheric conditions.

To evaluate the uptake coefficient, it is necessary to define the local concentration of HNO_3, since γ depends on [HNO_3]$^{1/2}$.

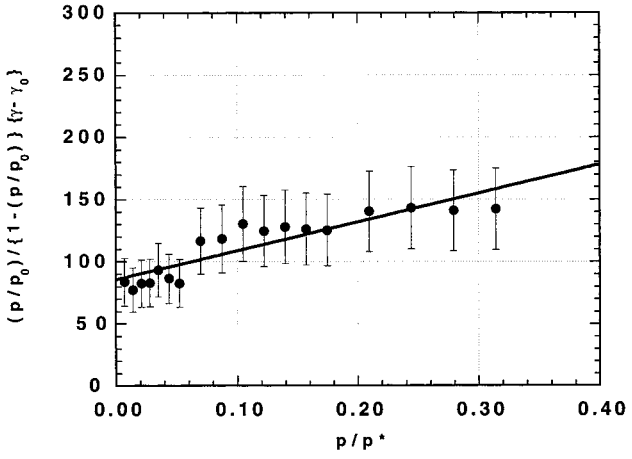

Figure 12. Plot of $\{z/(1 - z)\}\{\gamma - \gamma_o\}^{-1}$ against z ($z = p/p_0(H_2O)$ for the data obtained at $[HNO_3] = 6.0 \times 10^{-12}$ molecule cm^{-3}. γ_0 is the uptake coefficient obtained on "dry salt" for these conditions.

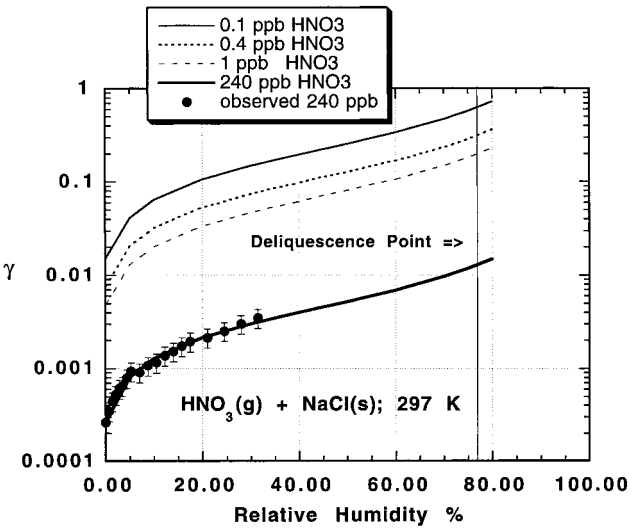

Figure 13. Dependence of γ with relative humidity for different HNO_3 concentrations relevent for the marine boundary layer at ambient temperature.

By use of the value of $k_sK_e^{1/2}$ based on our 298 K results and assuming that sea salt particles contain the same number of defect sites as microcrystalline NaCl powders used in laboratory work, a value of γ_m can be calculated from eq iv for any specified $[HNO_3]$ at this temperature. Equation vi can then be used to calculate γ as a function of relative humidity. Some examples of the dependence are shown in Figure 13. In a typical marine boundary layer influenced by aged continental air flow, $[HNO_3]$ may lie in the range 0.1−1.0 ppb (i.e., $(2.5-25) \times 10^9$ molecule cm^{-3} at 288 K). At 75% RH the corresponding γ lies in the range 0.2−0.6, i.e., approaching the diffusion-controlled regime.

By use of a typical surface area of the fine particle fraction of the sea salt aerosol in the open oceans of between 2 and 20 μm^2 cm^3, the "lifetime" of HNO_3 will be on the order of 1 h using $\gamma = 0.2$. In dryer, more polluted air masses, γ values will be lower and also reaction may be limited by availability of Cl^- if the aerosol becomes depleted. Nevertheless, it can be seen that this reaction will provide an important sink for gaseous HNO_3 in the marine environment, which will be competitive with the dry deposition of HNO_3 to the ocean surface. The reaction plays the role of converting NO_y into inorganic chlorine, in the form of HCl, which then provides a potential source of oxidized Cl^-, in the form of ClO, through the reactions

$$OH + HCl \rightarrow H_2O + Cl$$

$$Cl + O_3 \rightarrow ClO + O_2$$

This offers a route to HOCl, which, through its heterogeneous reactions, can lead to the release of further chlorine by the reactions

$$HO_2 + ClO \rightarrow HOCl + O_2$$

$$HOCl(aq) + Cl^- \rightarrow Cl_2 + OH^-$$

The extent to which these redox reactions occurs in the marine environment has yet to be assessed.

Conclusions

This study has shown that a rapid gas−solid reaction occurs with release of gaseous HCl when HNO_3 vapor is exposed to crystalline NaCl. After an initial period of decreasing surface reactivity, γ values under steady-state conditions decreased with increasing HNO_3 concentration and increased with H_2O over the range 0.002−10 mbar. The form of these dependencies could be explained in terms of a mechanism of the reaction $HNO_3(g) + NaCl(s) \rightarrow HCl(g) + NaNO_3(s)$, which involves ionic dissociation of adsorbed HNO_3 molecules in the presence of surface adsorbed water followed by reaction of H_3O^+ with Cl^- and desorption of HCl molecules. This mechanism involving ionic dissociation in the presence of surface adsorbed water may be an important first step in the heterogeneous reactions of other atmospheric gases that ionize in aqueous media, on atmospheric aerosols containing solid electrolytes.

Acknowledgment. The authors thank the U.K. Natural Environment Research Council and the Commission of the European Communities for support for this research. We also thank J. C. Mossinger and C. J. Percival, who helped with data collection and analysis.

References and Notes

(1) Singh, H. B.; Kasting, J. F. *J. Atmos. Chem.* **1988,** *7*, 261.
(2) Keene, W. C.; Pszenny, A. A. P.; Jacob, D. J.; Duce, R. A.; Galloway, J. N.; Schultz-Tokos, J. J.; Sievering, H.; Boatman, J. F. *Global Biogeochem. Cycles* **1990**, *4*, 407.
(3) Finlayson-Pitts, B. J. *Res. Chem. Intermed.* **1993**, *19*, 235.
(4) Jobson, B. T.; Niki, H.; Yokouchi, Y.; Bottenheim, J.; Hopper, F.; Leaitch, R. *J. Geophys. Res.* **1994**, *99*, 25355.
(5) Pszenny, A. A. P.; Keene, W. C.; Jacob, D. J.; Fan, S.; Maben, J. R.; Zetwo, M. P.; Springer-Young, M.; Galloway, J. N. *Global Biogeochem. Cycles* **1993**, *20*, 699.
(6) Blanchard, D. C.; Woodcock, A. H. *Ann. N.Y. Acad. Sci*. **1980,** *338*, 330.
(7) Eriksson, E. *Tellus* **1959**, *11*, 375.
(8) Duce, R. A. *J. Geophys. Res.* **1969**, *74*, 4597.
(9) Robbins, R. C.; Cadle, R. D.; Eckhardt, D. L. *J. Met*. **1959**, *16*, 53.
(10) Finlayson-Pitts, B. J.; Elzell, M. J.; Pitts, J. N., Jr. *Nature* **1989**, *337*, 241.
(11) Zetsch, C.; Pfahler, G.; Behnke, W. *J. Aerosol Sci.* **1988**, *19*, 1203.
(12) Vogt, R.; Crutzen, P. J.; Sander, R. *Nature* **1996**, *383*, 327.
(13) Sievering, H.; Ennis, G.; Gorman, E. *Global Biogeochem. Cycles* **1990**, *4*, 395.
(14) Fenter, F. F.; Caloz, F.; Rossi, M. J. *J. Phys. Chem.* **1994**, *98*, 9801.
(15) Laux, J. M.; Hemminger, J. C.; Finlayson-Pitts, B. J. *Geophys. Res. Lett.* **1994**, *21*, 1623.
(16) Fenter, F. F.; Caloz, F.; Rossi, M. J. *J. Phys. Chem.* **1996**, *100*, 1008.
(17) Leu, M.-T.; Timonen, R. S.; Keyser, L. F.; Yung Y. L. *J. Phys. Chem.* **1995**, *99*, 13203.
(18) Beichert, P.; Finlayson-Pitts, B. J. *J. Phys. Chem.* **1996**, *100*, 15218.
(19) Walter, H. U. *Z. Phys. Chem. Neue Folge* **1971**, *75*, 287.

(20) Kaiko, M.; Chikazawa, M.; Kanazawa, T. *Nippon Kagaku Kaishi* **1972**, *8*, 1386.
(21) Barraclough, P. B.; Hall, P. B. *Surf. Sci.* **1974**, *46*, 393.
(22) Brimblecombe, P.; Clegg, S. L. *J. Atmos. Chem.* **1988**, *7*, 1.
(23) Howard, C. J. *J. Phys. Chem.* **1979**, *83*, 3.
(24) Brown, R. L. *J. Res. Natl. Bur. Stand.* **1978**, *83*, 1.
(25) Keyser, L. F.; Moore, S. B.; Leu, M.-T. *J. Phys. Chem.* **1991**, *95*, 5496.
(26) Van Doren, J. M.; Watson, L. R.; Davidovits, P.; Worsnop, D. R.; Zahniser, M. S.; Kolb, C. E. *J. Phys. Chem.* **1990,** *94*, 3265.
(27) Dai, D. J.; Peters, S. J.; Ewing, G. E. *J. Phys. Chem.* **1995,** *99*, 10299.
(28) Folsch, S.; Stock, A.; Henzler, M. *Surf. Sci.* **1992**, *264*, 65.
(29) Laux J. M.; Fister, T. F.; Finlayson-Pitts, B. J.; Hemminger, J. C. *J. Phys. Chem.* **1996**, *100* 19891.
(30) Peters, S. J.; Ewing, G. E. *J. Phys. Chem.* **1996**, *100*, 14093.
(31) Timonen, R. S.; Keyser, L. F.; Yung Y. L. *J. Phys. Chem.* **1995**, *99*, 13203.
(32) Adamson, A. A. *Physical Chemistry of Surfaces*, 5th ed.; Wiley: New York, 1990.
(33) Atkins, P. W. *Physical Chemistry*, 6th ed.; Oxford University Press, 1998.
(34) Peters, S. J.; Ewing, G. E. *Langmuir* **1997**, *13*, 14093.